Journal of Alloys and Compounds 960 (2023) 170982

Contents lists available at ScienceDirect

Journal of Alloys and Compounds

journal homepage: www.elsevier.com/locate/jalcom

Enhanced mechanical properties and homogeneous T5 age-hardening behavior of Al-Si-Cu-Mg casting alloys

Hyeon-Woo Son [a,1], Ji-Young Lee [a,1], Young-Hee Cho [a], Jae-il Jang [b], Soo-Bae Kim [a], Jung-Moo Lee [a,*]

[a] Metallic Materials Division, Korea Institute of Materials Science, Changwon 51508, Republic of Korea
[b] Division of Materials Science and Engineering, Hanyang University, Seoul 04763, Republic of Korea

ARTICLE INFO

Article history:
Received 12 April 2023
Received in revised form 29 May 2023
Accepted 13 June 2023
Available online 15 June 2023

Keywords:
Al-Si-Cu-Mg alloy
T5 treatment
Melting temperature
Precipitate
Melt treatment

ABSTRACT

In this study, the effects of melt-holding temperatures on the mechanical properties and T5 age-hardening behavior of Al-Si-Cu-Mg alloys were investigated. An enhanced yield strength, tensile strength, and elongation were observed simultaneously as the melt-holding temperature was increased from 720 °C to 820 °C. The enhanced mechanical property of the T5-treated Al-Si-Cu-Mg alloy with high melt-holding temperature was attributed to several microstructural changes, including a refinement of the microstructure and an acceleration of the precipitation kinetics caused by enhanced second-phase dissolution. The high melt-holding temperature was particularly effective in changing the precipitation kinetics. This was demonstrated by the formation of a single peak upon homogenization of the solute distribution, replacing the double hardness peaks found in the Al-Si-Cu-Mg alloy with a low melt-holding temperature. The homogeneous solute distribution not only increased the number of Si- and β-type precipitates in the alloy with a high melt-holding temperature but also refined their size. In addition, the high melt-holding temperature accelerated the segregation behavior of Cu on the Si precipitates, which is critical for the refinement of precipitates.

1. Introduction

The Al-Si-Cu-Mg alloy system, which is suitable for heat treatment, is a representative high-strength casting alloy used for automobile parts. However, the conventional T6 heat treatment of Al-Si-Cu-Mg alloys, which consists of solution treatment and artificial aging, has recently encountered new challenges. Modern automotive components are becoming larger, thinner, and more complex, and require minimal exposure to high temperatures owing to distortion during quenching after solution heat treatment [1,2]. In addition, the environmental regulations on CO_2 emissions restrict high energy consumption. Therefore, T5 treatment has received considerable attention from the automobile industry because it does not involve solution heat treatment, thus solving both the distortion of automobile parts and environmental problems [3,4]. However, the inferior mechanical properties of T5-treated Al-Si-Cu-Mg alloys are a major concern, hindering their application in the automotive industry.

Although thermodynamic simulations and phase-field models have successfully predicted microstructures [5–7], experimental approaches remain popular as they enhance the mechanical properties of T5-treated Al-Si-Cu-Mg alloys by allowing effective control of inclusions and precipitates [8]. Hard inclusions, such as Si, Q-$Al_5Cu_2Mg_8Si_6$, θ-Al_2Cu, and β-Mg_2Si, are formed during the solidification of Al-Si-Cu-Mg alloys. The eutectic β-Mg_2Si phase exhibits excellent mechanical properties at room temperature [9]. However, many studies have shown that when the amount of Mg increases, the interaction with Fe, an impurity in Al alloys, forms a brittle π-$Al_8Mg_3FeSi_6$ phase that leads to inferior mechanical properties [10]. The Cu element in the Al-Si-Cu-Mg alloy contributes to the mechanical properties by forming Q-$Al_5Cu_2Mg_8Si_6$ and θ-Al_2Cu phases [11,12]. However, when the Q phase is present in excess, the mechanical properties of the alloy are degraded due to coarsening and segregation. Several reports also claim that the excessive addition of Cu leads to the generation of pores and the degradation of mechanical properties by hindering the feeding of Cu-rich phases during solidification [13].

* Corresponding author.
E-mail address: jmoolee@kims.re.kr (J.-M. Lee).
[1] These authors contributed equally to this work.

https://doi.org/10.1016/j.jallcom.2023.170982

Al-Si-Cu-Mg alloys can be strengthened by the following precipitation process after T6 heat treatment [14,15]:

SSSS → clusters → GP – zones → β″, L, C, QP, QC → β', Q' → Q

Precipitates at peak hardness during artificial aging of the Al-7Si-1.0Cu-0.5Mg alloy are known as β″and Q′ [11] or β″, Q′ and L precipitates [15]. A similar precipitation behavior is expected when the alloy is T5-heat-treated. However, the T5 treatment does not include a solid-solution heat treatment. Consequently, precipitation hardening is less likely to occur than with the T6 treatment as a higher number of inclusions remain in the matrix upon T5 treatment.

Therefore, the key to enhancing the mechanical properties of T5-treated Al-Si-Cu-Mg alloys is to dissolve the inclusions as much as possible in the as-cast state. Melt treatment (the control of melting) and solidification are methods commonly used to control the microstructure of as-cast alloys. In this context, several processes have been reported, including solidification rate [16], the use of an ultrasonic treatment [17,18], the use of inoculation [19,20], the addition of alloying elements [21], melting temperature [22], and the mixing of melts with different temperatures [23].

Of these processes, controlling the melt-holding temperature has the potential to simultaneously improve the strength and ductility of T5-treated Al-Si-Cu-Mg alloys [24–28]. Whereas some researchers have reported that high melting temperatures increase the grain size by reducing the number of nucleation sites [29], others have shown that they refine the shape of the Si phase from an irregular to an octahedral shape in hypereutectic alloys [30]. In addition, the microstructure becomes less sensitive to changes in the solidification rate, and therefore more controllable [31]. These results correspond with recent results that have shown the refinement of Mg_2Si from a skeleton to a polygonal shape with a reduction in size at a high melting temperature of 950 °C [27]. The most interesting finding of the studies that used superheating is that both strength and elongation can be enhanced by holding the melt at a high temperature for a relatively short time, and then cooling it to the pouring temperature of commercial Al alloys [32] The reason for the superior mechanical properties of melt-treated Al alloys is that Si–Si clusters dissolve better with increasing melt-holding temperatures [26]. The effect was particularly pronounced at the melting temperature of > 800 °C, where the atomic density and coordination number of Al alloys rapidly decrease. The above investigations suggest that dissolved solutes from clusters in a high-temperature melt can be maintained even if the melt temperature is decreased to the pouring temperature of commercial alloys. This means that T5-treated Al-Si-Cu-Mg alloys, which have inhomogeneous solute distributions owing to the absence of a solid-solution treatment, can be refined by temporarily holding the melt at high temperatures, thereby controlling the secondary phases and precipitates.

As stated above, high melt-holding temperature are expected to have positive effects in the T5 treatment. However, research on the effects of changing melt-holding temperatures in the T5 treatment is insufficient because previous studies have focused on the morphology and size distribution of the constituent phase particles rather than on the matrix. Therefore, this study mainly investigated the effects of melt treatment (melt-holding temperature) on T5-treated Al-Si-Cu-Mg alloys by analyzing their solute distribution and precipitation behavior.

Table 1
Chemical composition of Al-Si-Cu-Mg alloy.

Elements	Si	Cu	Mg	Fe	Mn	Sr	Al
(wt%)	7.17	1.15	0.50	0.12	0.18	100 ppm	Bal.

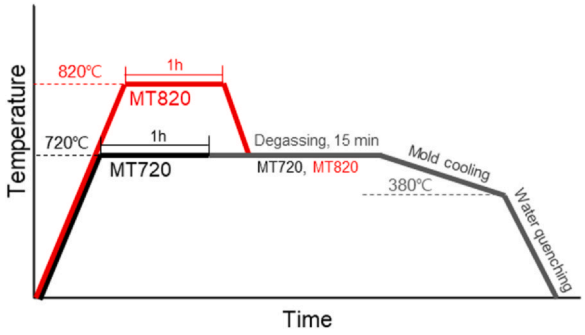

Fig. 1. Schematic of the T5 histories of MT720 and MT820.

2. Experimental

The Al-7Si-1Cu-0.5Mg alloys were prepared by melting 10 kg of commercial A356.2 alloy, pure Cu, and a master alloy of Al-15 wt% Mn and Al-10 wt% Sr. The alloy compositions are listed in Table 1. The alloys were melted and held at 720 °C (MT720) and 820 °C (MT820) for 1 h each in an electric resistance furnace. The melt-holding temperature of MT820 was then decreased to 720 °C, while that of MT720 was kept at 720 °C. Both melts were degassed with high-purity Ar gas, stabilized for 15 min, and then poured into a Cu book mold preheated to 180 °C. Thus, the cast samples were initially mold-cooled. Upon reaching 380 °C, the cast samples were removed from the mold and immediately water-quenched. Finally, the alloys were artificially aged at 190 °C (T5) for 16 h. The overall casting and heat-treatment process is represented in Fig. 1.

To evaluate the mechanical properties, the hardness of the specimens was measured at seven time points during the aging treatment, using a Vickers hardness tester. The hardness was measured under a load of 0.01 kgf and at a reduction time of 10 s, and the arithmetic average was calculated over five values (excluding the maximum and minimum values). The room-temperature tensile test was performed three times at a strain rate of 1×10^{-3} using rod-shaped ASTM-E8M sub-sized specimens to measure the yield strength (YS; 0.2% offset), tensile strength (TS), and elongation.

For microstructural characterization, the specimens were mechanically polished, and their macroscopic microstructures were analyzed using optical microscopy (OM), scanning electron microscopy (SEM), electron probe microanalysis (EPMA), and electron backscatter diffraction (EBSD). For the quantitative analysis of the phase distribution, OM and SEM images were analyzed using the I-Solution DT image analysis program to measure the fraction of each phase. The solute distribution within the matrix was measured by line-profile analysis of the EPMA, and the grain size was measured using the TSL-OIM software with EBSD data. To analyze the fine precipitates, specimens were prepared for transmission electron microscopy (TEM) using a focused ion beam (FIB). The specimens were observed using TEM accelerated at 200 kV along the $[100]_{Al}$ zone axis.

3. Results

3.1. As-cast microstructure

Fig. 2 shows the as-cast microstructure of the Al-Si-Cu-Mg alloy at different melt-holding temperatures. Typical dendritic α-Al and fibrous eutectic Si, caused by the addition of Sr, were observed in both MT720 and MT820. Whereas the eutectic area in MT720 appears predominantly course, a relative homogeneous eutectic structure was formed in MT820 (Fig. 2a and b). Fig. 2c and d show that the individual particles in the eutectic structure are much finer, whereas an increased secondary dendrite arm spacing (SDAS) is seen

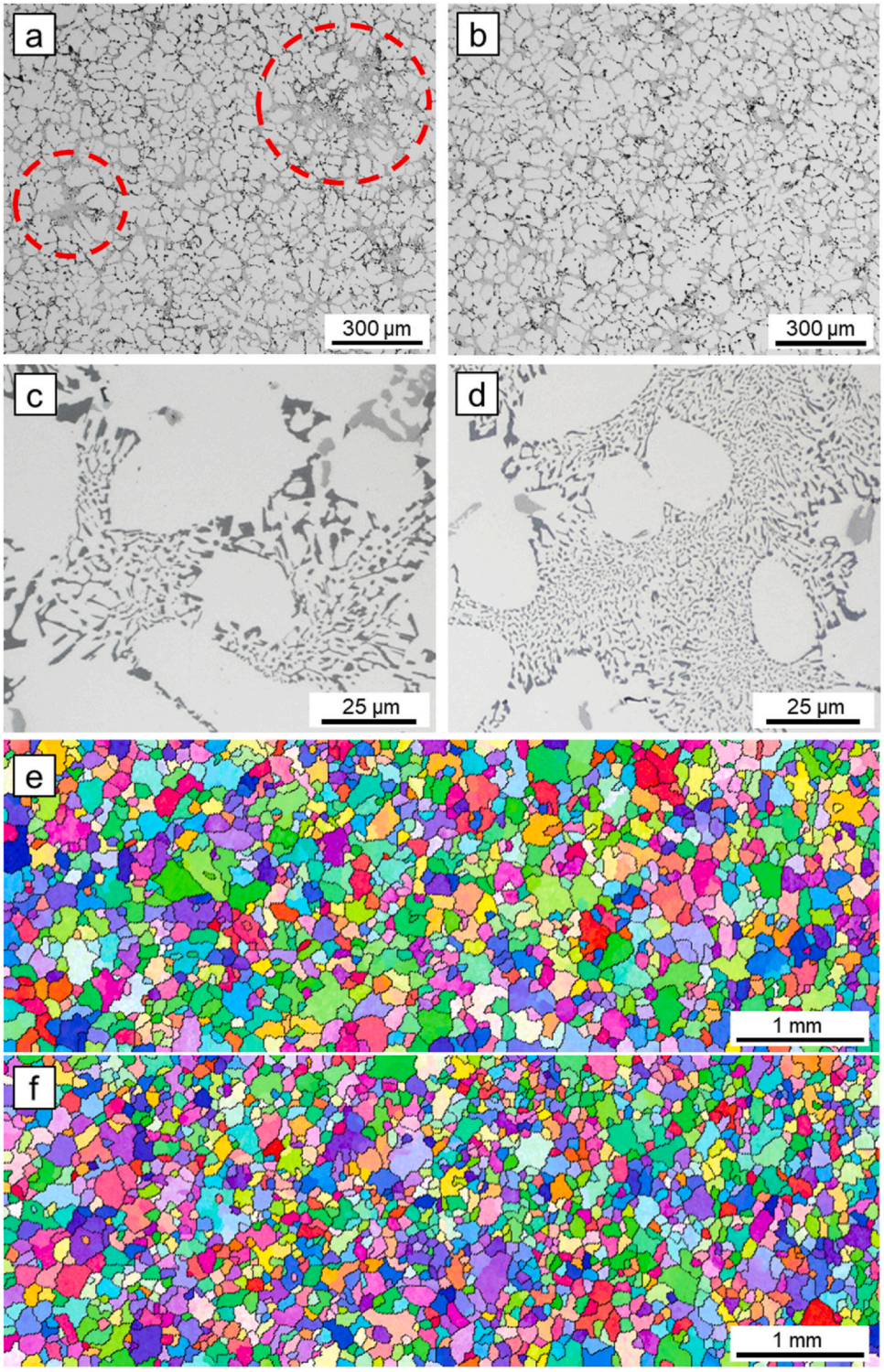

Fig. 2. (a-d) OM images and (e-f) IPF maps of the as-cast MT720 and MT820. The red circles in (a) indicate agglomerated eutectic structures.

at a high melt-holding temperature. The SDAS increased slightly from 30.8 μm to 36.7 μm with an increase in melting temperatures from 720 °C to 820 °C, whereas the average size of eutectic Si decreased from 1.85 μm to 1.00 μm. Lastly, inverse pole figure (IPF) maps of the two different specimens represent measurements of average grain sizes of 111.9 and 102.4 μm for MT720 and MT820, respectively. These results indicate that a high melt-holding temperature is effective in refining the grain size and eutectic structure.

Fig. 3 shows the phase analysis of the secondary phases of each alloy. Based on the phase analysis by OM and the backscatter diffraction (BSE) images (Fig. 3a and b), image analysis was conducted to measure the phase amount (Fig. 3c and d). Fig. 3e and f show the second-phase distributions of the alloys. The amounts of the Q, π, and Al_2Cu phases decrease when the melt-holding temperature is high, while those of the α-FeMn and Mg_2Si phases slightly increase. However, Fig. 3e indicates that the overall amount of the second phase decreased slightly when the melt-holding temperature was

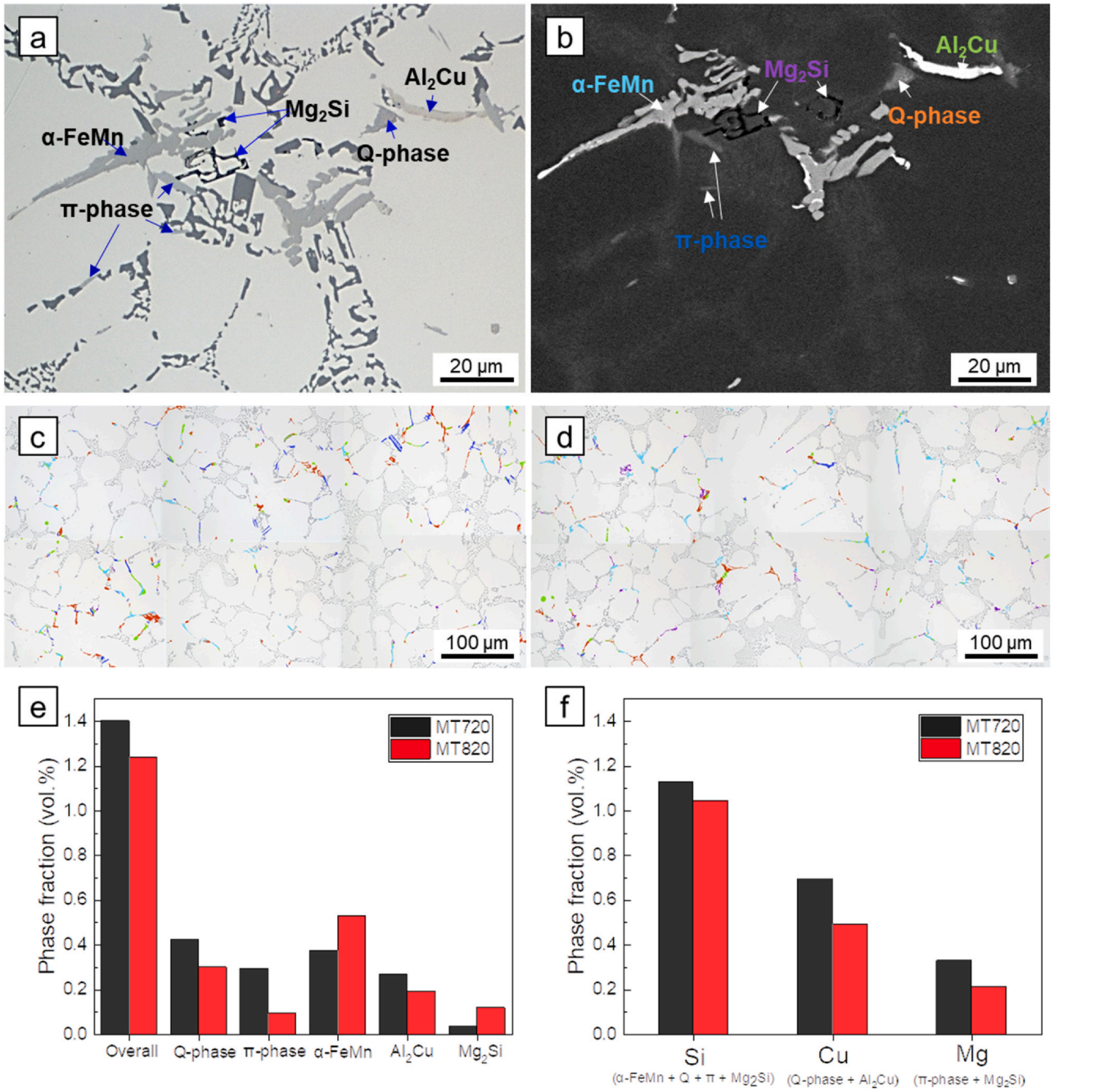

Fig. 3. (a-b) OM and SEM images representing the second-phase distribution; image processing to measure the phase fractions of (c) MT720 and (d) MT820; and the measured phase fractions according to the (e) phase type and (f) elements of the as-cast MT720 and MT820.

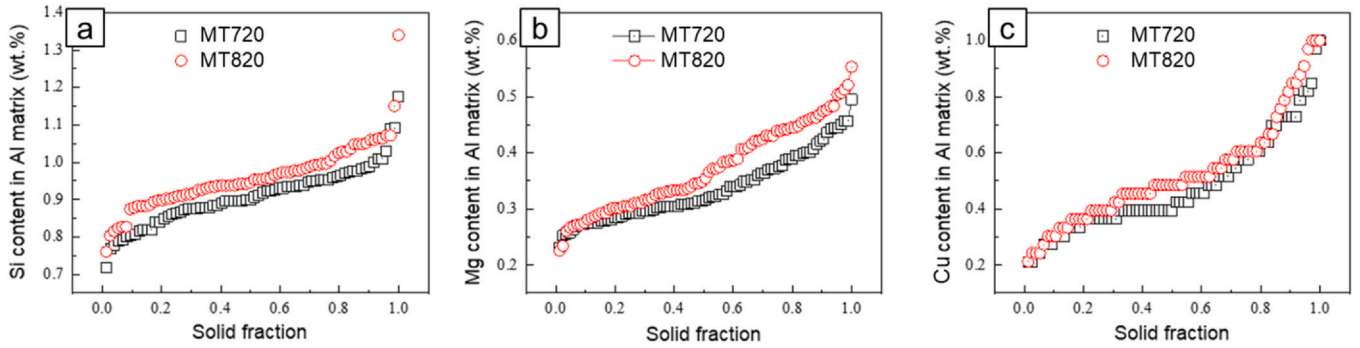

Fig. 4. EPMA line analysis of the solute distributions of (a) Si, (b) Mg, and (c) Cu in the Al matrix.

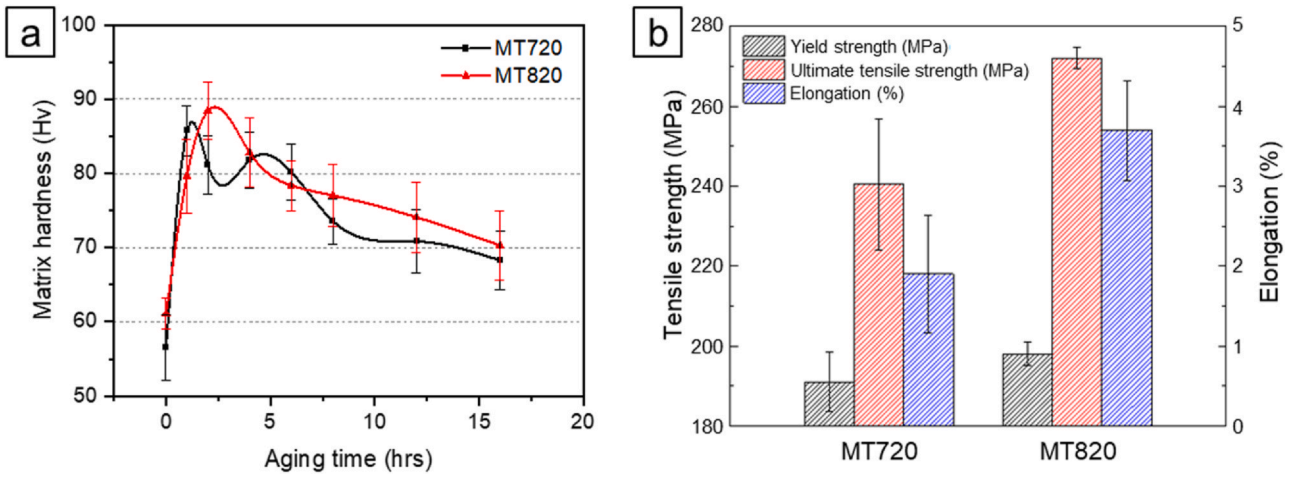

Fig. 5. (a) Hardness curves and (b) tensile properties of the T5-treated MT720 and MT820.

high. The decreased amounts of secondary phases containing Si, Cu, and Mg (Fig. 3f) imply that a high melt-holding temperature is effective in dissolving the secondary phases of Al-Si-Cu-Mg alloys, regardless of the secondary phase type.

The EPMA results in Fig. 4 show the solute concentration profiles of Si, Mg, and Cu in the Al matrix according to the solid fraction. The concentration profiles were measured by line-scanning electron probe microanalysis (EPMA) in the Al matrix of 10 dendritic cells. When the partition coefficients of Mg, Si, and Cu were less than 1, the solute concentrations increased with the solid fraction. The solute contents of Mg, Si, and Cu were higher in MT820 than in MT720, indicating that more solute is generated in the as-cast state when the melt is held at high temperatures.

3.2. Precipitation behavior

Fig. 5a and b show the T5-aging curves at 190 °C and the mechanical properties of the two melt-treated Al-Si-Cu-Mg alloys, MT720 and MT820. Fig. 5a shows that the higher melt-holding temperature increased the hardness in the entire aging history, with the peak hardness for MT720 and MT820 measured as 85.8 and 88.4 HV, respectively. However, the time required for peak aging was slightly shorter when the melt-holding temperature was low, taking only 1 h for MT720 and 2 h for MT820. A double-hardness peak is shown for MT720, with the first peak at 1 h with a hardness of 85.8 HV and the second peak at an aging time ranging from 4 h to 6 h with a hardness of 82.6 HV. Fig. 5b represents the tensile properties of the peak-aged MT720 and MT820, showing that a higher melt-holding temperature resulted in an increased YS, ultimate TS (UTS), and elongation. Tensile properties of 191.2 and 198.3 MPa (YS), 240.3 and 253.8 MPa (UTS), and 1.9% and 3.8% (elongation) were measured for MT720 and MT820, respectively.

The electrical conductivities of the alloys were used to interpret the precipitation kinetics based on the Avrami model. Since electrical conductivities typically decrease with the formation of atomic clusters and/or GP-zones while increasing with precipitation, they can be used to characterize precipitation kinetics [33,34]. The measured electrical conductivities of MT720 and MT820 (Fig. 6a) show an increase with increasing melt-holding temperature, regardless of the aging time. The electrical conductivities were used to calculate the fraction of transformed precipitate at a given time (t) using the following equation [35,36]:

$$f(t) = \frac{\frac{1}{\sigma_0} - \frac{1}{\sigma_t}}{\frac{1}{\sigma_0} - \frac{1}{\sigma_{max}}} \quad (1)$$

where $f(t)$ is the transformed fraction of the precipitate, σ_0 is the initial electrical conductivity, σ_t is the electrical conductivity at time t, and σ_{max} is the maximum electrical conductivity at the end of precipitation. Σ_{max} was assumed to be among the values measured in this study. The transformed fraction of the precipitate was described using the Avrami equation:

$$F(t) = 1 - \exp(-kt^n) \quad (2)$$

$$\ln(-\ln(1 - f(t))) = \ln(k) + n\ln(t) \quad (3)$$

where k and n are Avrami coefficients. Fig. 6b shows the Avrami plots for MT720 and MT820. Two precipitation stages, i.e., clustering and nucleation, were observed within the measured aging time ranges. The aging times of the conversion from clustering to nucleation were similar in MT720 (n = 0.72) and MT820 (n = 0.85). Whereas the fraction of transformed precipitates was slightly higher in MT720 early in the T5 treatment, MT820 showed a higher fraction of precipitates as the aging time increased. Moreover, the increased precipitation rate resulting from the high melting temperature was more prominent in the nucleation stage than in the clustering stage. The results of the precipitation kinetics indicate that precipitation is strongly favored by a higher melt-holding temperature.

Fig. 7 shows the bright-field (BF) TEM images of the peak-aged MT720 and MT820, obtained along the $[100]_{Al}$ zone axis. Fig. 7a and b display two types of precipitates: a gray needle-type β′ or β″ precipitate elongated into the [100] direction and a black rod-type Si precipitate. Table 2 presents the size and number density distributions for the precipitates, measured on the basis of the TEM images. MT820 yielded more and much finer precipitates than MT720, demonstrating that a high melt-holding temperature was effective in refining the precipitates while increasing their total amounts.

To analyze the precipitates in detail, atomic-scale high-angle annular dark-field scanning transmission electron microscopy (HAADF-STEM) images were obtained (Fig. 8). The overview image of HAADF-STEM in Fig. 8a shows that many precipitates of Si- and β-type phases have an atomic layer. The Si precipitate was observed to have the following orientation relationship with a coherent interface with the Al matrix: Si[110] // Al[001], with a size distribution ranging from 5 nm to 30 nm [37]. The B′′ precipitate, which has a β′′[100] // Al[100] orientation relationship, shows size ranges from 2 nm to 5 nm in radius and from 50 nm to 100 nm in length. Interestingly, most of the Si- and β-type precipitates had fine atomic layers with a high Z-contrast at the matrix interface. In addition, a Q′ precipitate containing a hexagonal network of Cu was detected, although the number density was too low to interpret the role of Cu. Energy-dispersive spectroscopy (EDS) indicated the presence of Cu. More

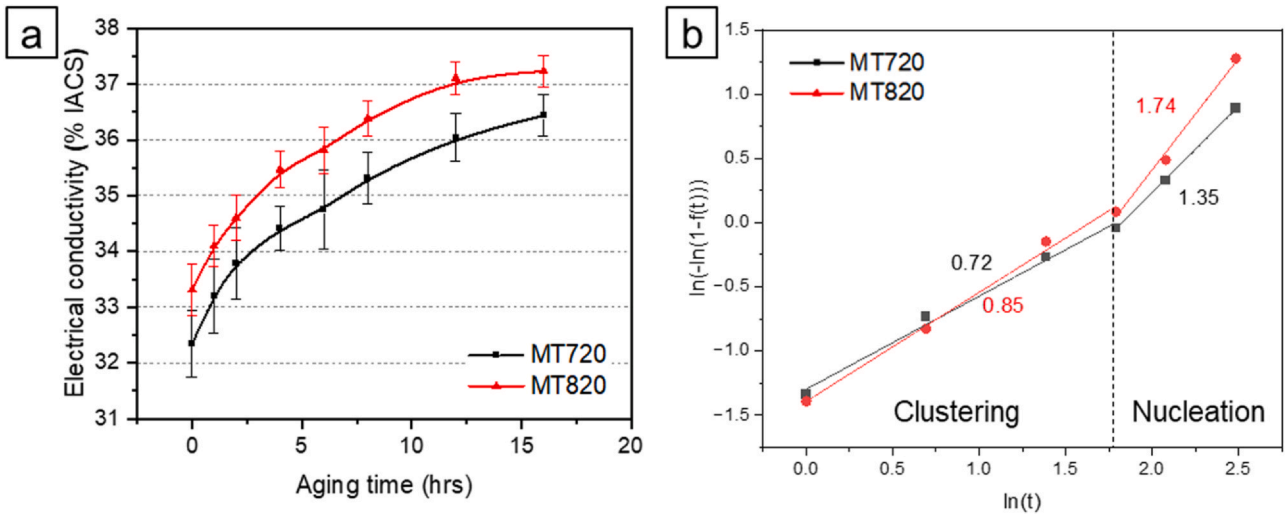

Fig. 6. (a) Electrical conductivity and (b) Avrami plots for precipitation kinetics of T5-treated MT720 and MT820. The numbers displayed in (b) indicate slopes.

specifically, the EDS maps in Fig. 9 show a fine atomic layer with a high Z-contrast at the interface, composed of Cu and Mg. The co-segregation of Cu and Mg at the interface of the Si precipitate suggests that Cu predominantly exists as a segregated layer at the interface of the β-type precipitate rather than generating Q′ precipitate when the Si precipitate expels Mg content from β-type precipitates.

4. Discussion

4.1. Factors contributing to Al-Si-Cu-Mg alloys strength

Considering the trend of reducing the number of automobile parts, this study showed that the T5 treatment can be applied for commercial use by controlling the melt treatment. The results of this study also suggested that the strength and elongation of T5-treated Al-Si-Cu-Mg alloys can be simultaneously enhanced by temporarily maintaining the melt at high temperatures [32]. Several factors affect the mechanical properties of melt-treated Al-Si-Cu-Mg alloys, including the SDAS, grain size, eutectic Si, and precipitation hardening. The following YS model represents the strength of a metallic material [38]:

$$\sigma = \sigma_0 + \sigma_d + \sigma_p + \sigma_{gb} + \sigma_s \quad (4)$$

where σ_d (10 MPa) is the Peierls–Nabarro stress [39], σ_d is the dislocation strengthening, σ_p is the precipitation strengthening, σ_{gb} is the grain boundary strengthening, and σ_s is the solid solution strengthening. Among the factors affecting overall strength, σ_{gb} and σ_p can be regarded as the main strengthening factors for the T5 peak-aged MT720 and MT820.

The contribution of grain refinement and SDAS variation to the strength is represented by the following Hall–Petch equation:

$$\sigma_{gb} = k_{hp} d^{-0.5} \quad (5)$$

where k_{hp} (0.068 MPa·m$^{1/2}$) is the Hall–Petch constant [38] and d is the crystallite size determined by the grain boundary and SDAS. The differences in YS caused by variations in SDAS and grain size were − 1.2 and 0.35 MPa for MT720 and MT820, respectively. Therefore, the strength variation due to the change in grain size caused by the melt treatment was insignificant to the mechanical properties of the Al-Si-Cu-Mg alloy.

The strengths of the T5 peak-aged MT720 and MT820 with nanoprecipitate structures were dominated by the dislocation–bypassing mechanism. The contribution of the precipitate to the strengths of MT720 and MT820 is represented by the Orowan–Ashby equation [40], as follows:

$$\sigma_p = \frac{0.13Gb}{L} \ln \frac{r}{b} \quad (6)$$

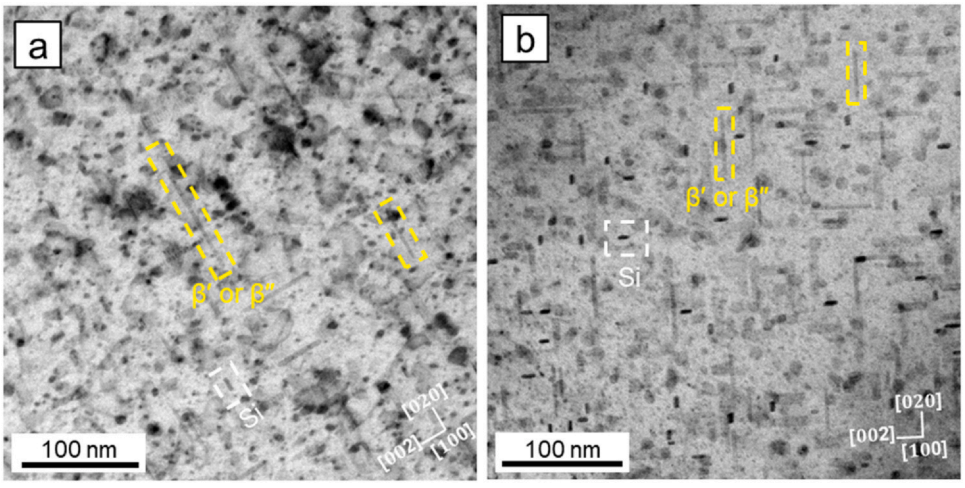

Fig. 7. TEM micrographs of (a) MT720 and (b) MT820 obtained along the $[100]_{Al}$ zone axis.

Table 2
Size (diameter) and number density of precipitates in T5 peak-aged MT720 and MT820.

Precipitates	Size		Number density	
	MT720	MT820	MT720	MT820
Si	11.1 ± 1.7 nm	9.2 ± 1.5 nm	1.3×10^{-4} nm^{-2}	2.6×10^{-4} nm^{-2}
β″ or β′	44.4 ± 15.8 nm	37.2 ± 10.5 nm	1.9×10^{-4} nm^{-2}	2.5×10^{-4} nm^{-2}

where G(26.9GPa) is the shear modulus of Al [41], b(0.29nm) is the Burgers vector, r is the average radius of the precipitate, and L is the average spacing between precipitates. L is represented by Eq. (7) [42]:

$$L = \left(\frac{2\pi}{f}\right)^{1/2} r, \tag{7}$$

where f is the volume fraction of the precipitate. Using Eq. (6) and the size and number density of Si and β-type precipitates represented in Table 2, the contributions of the precipitates on the strength were calculated as σ_p^{Si}= 24.1 MPa and $\sigma_p^{\beta-type}$= 42.9 MPa for MT720, and σ_p^{Si}= 32.0 MPa and $\sigma_p^{\beta-type}$= 47.2 MPa for MT820. A strength of 12.2 MPa can therefore be attributed to the precipitate, which increased with a change in melt-holding temperature from 720 ℃ to 820 ℃. This result shows that strengthening by precipitation is more dominant than strengthening by grain boundaries in T5-treated Al-Si-Cu-Mg alloys. Moreover, Eq. (6) was used to demonstrate that the superior strength of MT820 enhanced the precipitation of both Si- and β-type precipitates.

4.2. Effect of the melt treatment on precipitation behavior

Solute analysis also suggests that precipitation significantly contributes to the mechanical properties of T5-treated Al-Si-Cu-Mg alloys with melt treatment, such as T6 treatment. The decreased number of secondary phases in MT820 (Fig. 3e and f) and the increase in solute content measured by EPMA (Fig. 4) indicate that temporarily holding the melt at high temperatures is effective in dissociating the secondary phases in the melt of the Al-Si-Cu-Mg alloys. This result corresponds to the high number density of the precipitate (Fig. 7c) and the precipitation kinetics in the T5-treated MT820. Therefore, the significant change in the age-hardening response of the T5 treatment in MT820 was attributed to the large

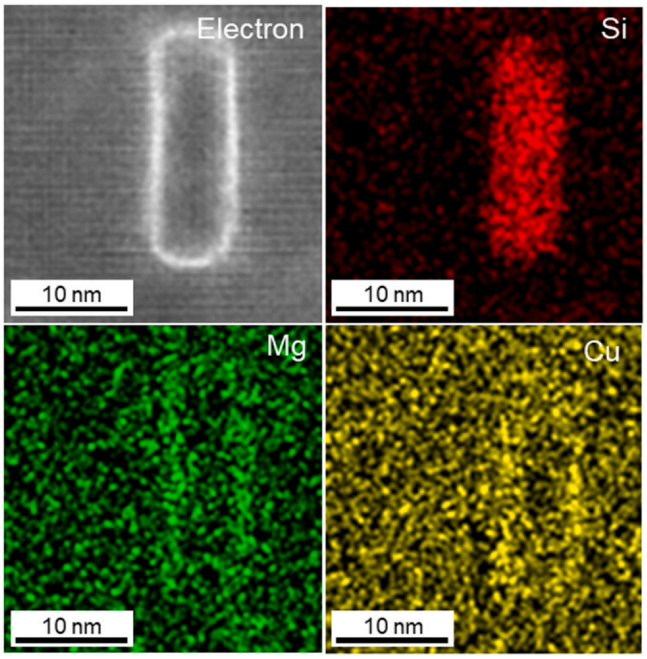

Fig. 9. EDS maps representing the co-segregation of Mg and Cu on the Si precipitate.

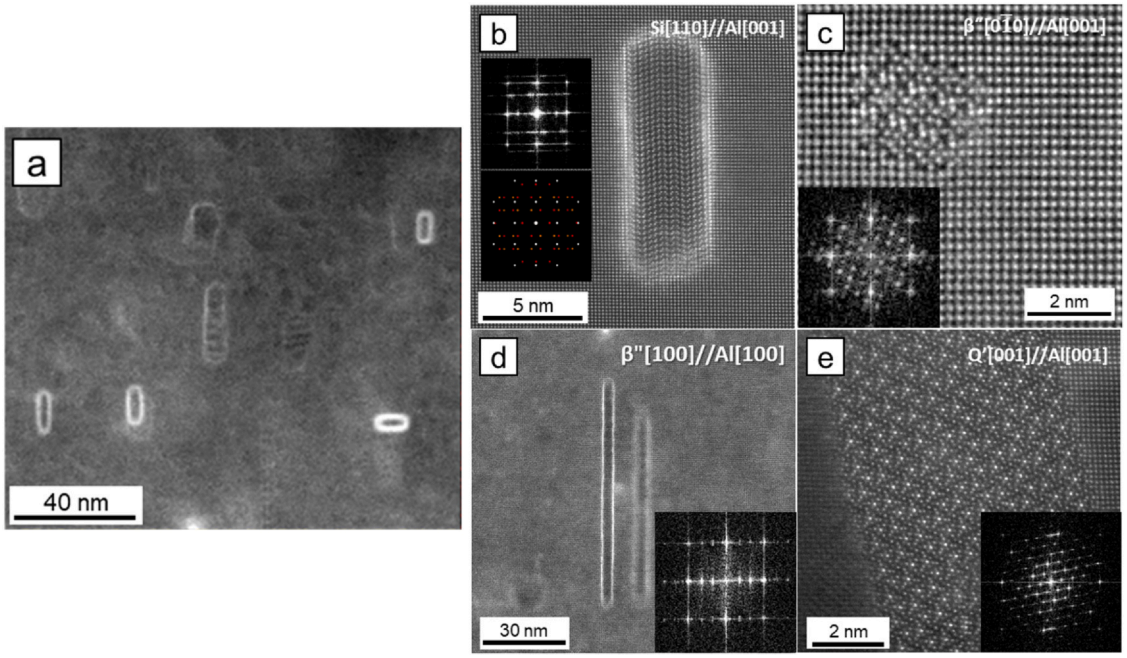

Fig. 8. (a) Overview image of HAADF-STEM and (b-e) magnified images representing the nanostructure of the precipitates in MT820. All TEM images were obtained along the $[100]_{Al}$ zone axis.

dissolution of dispersion that occurred during the melt-holding process at high temperatures.

The double- and single-peak formations in the hardness variations of MT720 and MT820 (Fig. 5a), respectively, also provide evidence for the different precipitation kinetics in MT720 and MT820. Although some points are within the error range, the overall hardness distribution indicates a difference in homogeneity between MT720 and MT820. Double-peak formation in MT720 is possibly related to an inhomogeneous solute distribution. In the case of the T5 heat treatment, which involves no homogenization process, the initial cluster distribution can be affected by the melt-holding temperature. Using a θ–θ type liquid metal X-ray diffractometer, Bian et al. reported that Si–Si cluster bonds break and dissolve into Al melt when the melt-holding temperature increases to 775 °C in Al-Si alloy melt [26]. In addition, when the melt-holding temperature increases from 775 °C to 875 °C, the mean atomic density and coordination number rapidly decrease. The report by Bian implies that high melt-holding temperatures effectively break the atomic bonding of clusters and homogeneously dissipate solute atoms in Al melt, particularly when the melt-holding temperature is > 800 °C. Therefore, it is quite likely that the as-cast MT720 had many clusters and an inhomogeneous solute distribution in its initial state, as the melt-holding temperature was below 800 °C. Conversely, the single hardness peak in the MT820 implies a homogeneous solute distribution in the as-cast MT820 alloy. The observation that the time required to reach the first peak hardness was much shorter in MT720 supports the inference stated above because inhomogeneity can locally accelerate precipitation hardening. However, this does not mean that the overall precipitation kinetics were much faster in MT720. If that had been the case, one would not have expected a second hardness peak at a later stage of the T5 treatment. The results of the Avrami kinetics also demonstrate that the precipitation kinetics were not significantly faster for MT720 than for MT820 (Fig. 6).

Only a limited number of studies have been conducted on cluster formation in melts. Further research is thus required to determine whether factors such as solute distribution and/or cluster formation affect double-peak formation. Although the effects of clusters on artificial aging are controversial, Røyset et al. reported that clusters formed during natural aging retard the subsequent artificial aging when Mg + Si > 1 wt% [43,44]. Considering the high Mg + Si wt% used in this study, the first peak hardness in MT720 may be attributed to rapid precipitation at a region of highly concentrated solute, while the second peak hardness appears to have resulted from the transformation of clusters into hardened precipitates. Recent studies have suggested that the earliest clusters are mainly composed of Si-rich Mg-Si co-clusters, implying that Al-Si base casting alloys with very high Si concentrations may have abundant Si-rich aggregates in the as-cast state [45]. A high melt-holding temperature is known to break Si–Si bonds. It is thus expected that an increase in melt-holding temperatures will be highly effective in homogenizing the solute, particularly in Al-Si base-casting alloys [26,46,47].

The segregation of Cu on the Si- and β-type precipitates (Fig. 9) is also seemingly related to the high melt-holding temperature. The reduction in Cu-bearing inclusions shown in Fig. 3f indicates that Cu segregation is much stronger in MT820. Several reports have suggested that Cu segregates at the interface of the precipitate, hindering its growth by reducing the interfacial strain energy [48,49]. Saito et al. have found that Cu segregation at the β″/Al interface removes misfit dislocations normally formed at the interface of β″ [49]. The high content of Cu solutes in MT820 seems to have suppressed the growth of Si, β-type precipitates more effectively. In conclusion, a high melt-holding temperature accelerates the overall precipitation kinetics by reducing the inhomogeneity of the solute distribution and refining the microstructure of T5-treated Al-Si-Cu-Mg alloys by providing a high solute concentration.

5. Conclusions

This study investigated the effects of melt-holding temperature on the T5 age-hardening behavior of Al-Si-Cu-Mg casting alloys. The results are summarized as follows.

(a) When the melt-holding temperature was increased from 720 °C (MT720) to 820 °C (MT820), several microstructural changes occurred in the as-cast state: (i) the sizes of the eutectic Si and grain decreased, (ii) the phase amounts of all inclusions that contained Si, Mg, and Cu decreased, and (iii) and the overall solute concentrations of Si, Mg, and Cu increased.
(b) The YS, TS, and elongation were remarkably enhanced with an increase in melt-holding temperature, indicating that the trade-off between strength and elongation can be overcome by controlling melt-holding temperatures.
(c) The T5 age-hardening response significantly changed as the melt-holding temperature increased. The double-peak formation observed for MT720 was eliminated in MT820, indicating that a high melt-holding temperature homogenized the age-hardening response and solute distribution.
(d) The number density of Si- and β-type precipitates increased with an increase in melt-holding temperature, whereas the size of the precipitates decreased. The high number density was attributed to the high solute concentration, whereas the decrease in the size of the precipitates was attributed to enhanced Cu segregation, which is known to remove misfit dislocations at the interface.

CRediT authorship contribution statement

Hyeon-Woo Son: Writing – original draft, Writing – review & editing. **Ji-Young Lee**: Visualization, Investigation, Validation, Data curation. **Young-Hee Cho**: Visualization, Investigation. **Jae-il Jang**: Conceptualization, Methodology, Software. **Soo-Bae Kim**: Visualization, Investigation. **Jung-Moo Lee:** Funding, Supervision, Writing – review & editing.

Data Availability

No data was used for the research described in the article.

Declaration of Competing Interest

The authors declare that they have no known competing financial interests or personal relationships that could have appeared to influence the work reported in this paper.

Acknowledgements

This work was supported by the Civil Military Technology Cooperation Program (No. 21-CM-EC-08), funded by the Ministry of Trade, Industry, and Energy (MOTIE, Korea) and the Defense Acquisition Program Administration (DAPA, Korea), and supported by the Industrial Technology Innovation Program (No. 20012145), funded by MOTIE.

References

[1] R.N. Lumley, R.G. Odonnell, D.R. Gunasegaram, M. Givord, Heat treatment of high-pressure die castings, Metall. Mater. Trans. A 38 (2007) 2564–2574.
[2] K. Fukasawa, R. Mohri, T. Ohtake, T. Inoue, A. Kuroda, H. Kambe, M. Yoshida, Effect of Mn addition on the age-hardening behavior of an Al-(9–10)%Si-0.3%Mg die casting alloy in T5 and T6 heat treatment, Mater. Trans. 57 (2016) 959–965.
[3] N.P.E. Utami, H. Chandra, Mechanical properties analysis of Al-9Zn-5Cu-4Mg cast alloy by T5 heat treatment, Matec. Web Conf. 101 (2017) 01009.
[4] G.S. Peng, X.Y. Fu, Y.C. Gu, G.S. Song, S.S. Chen, Q.Q. Sun, W.D. Hua, Microstructural evolution and strengthening behavior of high-pressure die-cast

high-Cu Al-Si-Cu-Mg alloy with T5 treatment, J. Mater. Eng. Perform. 31 (2022) 5432–5440.
[5] L.Q. Chen, Y. Zhao, From classical thermodynamics to phase-field method, Prog. Mater. Sci. 124 (2022) 100868.
[6] Y. Zhao, Co-precipitated Ni/Mn shell coated nano Cu-rich core structure: a phase-field study, J. Mater. Res. Tech. 21 (2022) 546–560.
[7] K. Guo, G. Gou, H. Lv, M. Shan, Jointing of CFRP/5083 aluminum alloy by induction brazing: processing, connecting mechanism, and fatigue performance, Coatings 12 (10) (2022) 1559.
[8] S.B. Kim, J.M. Lee, T.M. Koo, S.U. Lee, J.Y. Lee, K.S. Son, Y.H. Cho, Influence of cooling condition after solidification on T5 heat treatment response of hypoeutectic Al-7Si-0.4Mg casting alloy, J. Alloy. Compd. 906 (2022) 164339.
[9] X. Zhu, X. Dong, P. Blake, S. Ji, Improvement in as-cast strength of high pressure die-cast Al-Si-Cu-Mg alloys by synergistic effect of Q-Al5Cu2Mg8Si6 and θ-Al2Cu phases, Mater. Sci. Eng. A 802 (2021) 140612.
[10] A.R. Farkoosh, M. Pekguleryuz, Enhanced mechanical properties of an Al-Si-Cu-Mg alloy at 300 °C: Effects of Mg and the Q-precipitate phase, Mater. Sci. Eng. A 621 (2015) 277–286.
[11] Y.J. Li, S. Brusethaug, A. Olsen, Influence of Cu on the mechanical properties and precipitation behavior of AlSi7Mg0.5 alloy during aging treatment, Scr. Mater. 54 (2006) 99–103.
[12] L. Zuo, B. Ye, J. Feng, X. Kong, H. Jiang, W. Ding, Effect of Q-$Al_5Cu_2Mg_8Si_6$ phase on mechanical properties of Al-Si-Cu-Mg alloy at elevated temperature, Mater. Sci. Eng. A 693 (2017) 26–32.
[13] H. Yang, S. Ji, W. Yang, Y. Wang, Z. Fan, Effect of Mg level on the microstructure and mechanical properties of die-cast Al–Si–Cu alloys, Mater. Sci. Eng. A 642 (2015) 340–350.
[14] C.D. Marioara, S.J. Andersen, T.N. Stene, H. Hasting, J. Walmsley, A.T.J. Van Helvoort, R. Holmestad, The effect of Cu on precipitation in Al–Mg–Si alloys, Philos. Mag. 87 (2007) 3385–3413.
[15] E.A. Mørtsell, F. Qian, C.D. Marioara, Y. Li, Precipitation in an A356 foundry alloy with Cu additions - a transmission electron microscopy study, J. Alloy. Compd. 785 (2019) 1106–1114.
[16] E. Lee, B. Mishra, Effect of cooling rate on the mechanical properties of AA365 aluminum alloy heat-treated under T4, T5, and T6 conditions, Int. J. Met. 12 (2018) 449–456.
[17] J. Nampoothiri, I. Balasundar, B. Raj, B.S. Murty, K.R. Ravi, Porosity alleviation and mechanical property improvement of strontium modified A356 alloy by ultrasonic treatment, Mater. Sci. Eng. A 724 (2018) 586–593.
[18] J.G. Jung, T.Y. Ahn, Y.H. Cho, S.H. Kim, J.M. Lee, Synergistic effect of ultrasonic melt treatment and fast cooling on the refinement of primary Si in a hypereutectic Al-Si alloy, Acta Mater. 144 (2018) 31–40.
[19] R.G. Guan, D. Tie, A review on grain refinement of aluminum alloys: progresses, challenges and prospects, Acta Metall. Sin. (Engl. Lett.) 30 (2017) 409–432.
[20] G.K. Sigworth, The modification of Al-Si casting alloys: important practical and theoretical aspects, Int. J. Met. 2 (2008) 41.
[21] S. Seifeddine, S. Johansson, I.L. Svensson, The influence of cooling rate and manganese content on the β-Al5FeSi phase formation and mechanical properties of Al-Si-based alloys, Mater. Sci. Eng. A 490 (2008) 385–390.
[22] C.L. Xu, Q.C. Jiang, Morphologies of primary silicon in hypereutectic Al-Si alloys with melt overheating temperature and cooling rate, Mater. Sci. Eng. A 437 (2006) 451–455.
[23] S. Manani, A.K. Pradhan, Effects of melt thermal treatment on cast Al-Si alloys: a review, Mater. Today-Proc. 62 (2022) 6568–6572.
[24] S.W. Hudson, D. Apelian, Inclusion detection in molten aluminum: current art and new avenues for in situ analysis, Int. J. Met. 10 (2016) 289–305.
[25] V. Fallah, B. Langelier, N. Ofori-Opoku, B. Raeisinia, N. Provatas, S. Esmaeili, Cluster evolution mechanisms during aging in Al–Mg–Si alloys, Acta Mater. 103 (2016) 290–300.
[26] X. Bian, W. Wang, Thermal-rate treatment and structure transformation of Al–13 wt% Si alloy melt, Mater. Lett. 44 (2000) 54–58.
[27] N.A. Nordin, T. Abubakar, E. Hamzah, S. Farahany, A. Ourdjini, Effect of superheating melt treatment on Mg2Si particulate reinforced in Al-Mg2Si-Cu In situ composite, Proc. Eng. 184 (2017) 595–603.
[28] Q.D. Qin, Y.G. Zhao, Y.H. Liang, W. Zhou, Effects of melt superheating treatment on microstructure of Mg2Si Al–Si–Cu composite, J. Alloy. Compd. 399 (2005) 106–109.
[29] R. Venkataramani, R. Simpson, C. Ravindran, Effect of melt superheat on maximum nuclei density in A356 alloy, Mater. Charact. 35 (1995) 81–92.
[30] C.L. Xu, Q.C. Jiang, Morphologies of primary silicon in hypereutectic Al–Si alloys with melt overheating temperature and cooling rate, Mater. Sci. Eng. A 437 (2006) 451–455.
[31] P. Li, V.I. Nikitin, E.G. Kandalova, K.V. Nikitin, Effect of melt overheating, cooling and solidification rates on Al–16wt%Si alloy structure, Mater. Sci. Eng. A 332 (2002) 371–374.
[32] H. Wang, B. Li, J. Jie, Z. Wei, Influence of thermal rate treatment and low temperature pouring on microstructure and tensile properties of AlSi7Mg alloy, Mater. Des. 32 (2011) 2992–2996.
[33] A. Bahrami, M.Y. Mehr, Modeling electrical resistivity of naturally aged Al-Mg-Si alloys, Metals 9 (3) (2019) 2019 310.
[34] O. Djema, M. Bouabdallah, R. Badji, A. Saadi, N. Kherrouba, A. Sahli, Isothermal and non-isothermal precipitation kinetics in Al-Mg-Si-(Ag) alloy, Mater. Chem. Phys. 240 (2019) 122073.
[35] J. Røyset, N. Ryum, Kinetics and mechanisms of precipitation in an Al–0.2wt% Sc alloy, Mater. Sci. Eng. A 396 (2005) 409–422.
[36] D.S. Yoshikawa, L.G. Carvalho, R.L. Plaut, A.F. Padilha, Effect of casting mode and thermal treatments on the electrical conductivity of the AA4006 aluminum alloy, REM, Int. Eng. J. 70 (2017) 471–476.
[37] S.J. Andersen, C.D. Marioara, R. Vissers, A. Frøseth, H.W. Zandbergen, The structural relation between precipitates in Al-Mg-Si alloys, the Al-matrix and diamond silicon, with emphasis on the trigonal phase U1-$MgAl_2S_2$, Mater. Sci. Eng. A 444 (2007) 157–169.
[38] H.X. Jiang, S.X. Li, Q.J. Zheng, L.L. Zhang, J. He, Y. Song, C.K. Deng, J.Z. Zhao, Effect of minor lanthanum on the microstructures, tensile and electrical properties of Al-Fe alloys, Mater. Des. 195 (2020) 108991.
[39] R.Z. Valiev, M.Yu Murashkin, I. Sabirov, A, nanostructural design to produce high-strength Al alloys with enhanced electrical conductivity, Scr. Mater. 76 (2014) 13–16.
[40] Z. Zhang, D.L. Chen, Consideration of Orowan strengthening effect in particulate-reinforced metal matrix nanocomposites: a model for predicting their yield strength, Scr. Mater. 54 (2006) 1321–1326.
[41] X. Sauvage, E.V. Bobruk, Y. M.Yu. Murashkin, N.A. Nasedkina, R.Z. Enikeev, Valiev, Optimization of electrical conductivity and strength combination by structure design at the nanoscale in Al-Mg-Si alloys, Acta Mater. 98 (2015) 355–366.
[42] S. Esmaeili, D.J. Lloyd, W.J. Poole, A yield strength model for the Al-Mg-Si-Cu alloy AA6111, Acta Mater. 51 (2003) 2243–2257.
[43] J. Røyset, T. Stene, J.A. Sæter, O. Reiso, The effect of intermediate storage temperature and time on the age hardening response of Al-Mg-Si alloys, Mater. Sci. Forum 519– 521 (2006) 519.
[44] F.A. Martinsen, F.J.H. Ehlers, M. Torsæter, R. Holmestad, Reversal of the negative natural aging effect in Al-Mg-Si alloys, Acta Mater. 60 (2012) 6091–6101.
[45] V. Fallah, B. Langelier, N. Ofori-Opoku, B. Raeisinia, N. Provatas, S. Esmaeili, Cluster evolution mechanisms during aging in Al-Mg-Si alloys, Acta Mater. 103 (2016) 290–300.
[46] Q.L. Wang, H.R. Geng, M. Zuo, F. Long, X. Peng, Effects of melt thermal rate treatment and modification of P and RE on hypereutectic Al-Si-Cu-Mg alloy, Mater. Sci. Tech. 29 (2013) 1233–1240.
[47] P. Li, V.I. Nikitin, E.G. Kandalova, K.V. Nikitin, Effect of melt overheating, cooling and solidification rates on Al–16wt%Si alloy structure, Mater. Sci. Eng. A 332 (2002) 371–374.
[48] K. Matsuda, D. Teguri, Y. Uetani, T. Sato, S. Ikeno, Cu-segregation at the Q′/α-Al interface in Al-Mg-Si-Cu alloy, Scr. Mater. 47 (2002) 833–837.
[49] T. Saito, F.J.H. Ehlers, W. Lefebvre, D. Hernandez-Maldonado, R. Bjørge, C.D. Marioara, S.J. Andersen, E.A. Mørtsell, R. Holmestad, Cu atoms suppress misfit dislocations at the β″/Al interface in Al-Mg-Si alloys, Scr. Mater. 110 (2016) 6–9.